J. Phys.: Condens. Matter 6 (1994) 4395–4404. Printed in the UK

Focusing and superfocusing effects in x-ray absorption fine structure at the iron K edge in FeF_3

A Kuzmin† and Ph Parent‡

† Institute of Solid State Physics, University of Latvia, Kengaraga 8, 1063 Riga, Latvia

‡ LURE, Université de Paris-Sud, Bâtiment 209D, 91405 Orsay Cédex, France

Received 3 September 1993, in final form 15 March 1994

Abstract. We present an *ab initio* multiple-scattering (MS) analysis of the Fe K-edge x-ray absorption fine structure (XAFS) in FeF_3 having a rhombohedrally distorted ReO_3-like structure. Good agreement between theoretical and experimental data was found in the energy range 2.5–14.0 $Å^{-1}$. It is shown that the MS contribution influences strongly the XAFS signals from atoms located beyond the first coordination shell. In particular (i) the XAFS signal from iron atoms Fe_2 in the second shell is amplified due to the focusing effect within the Fe_0–F_1–Fe_2 chains, caused by fluorine atoms F_1 of the first shell (Fe_0 denotes the absorber, and the number is related to the coordination shell); (ii) the contribution from iron atoms Fe_{21}, located as far as at 7.5 Å, is observed due to the 'superfocusing' effect within the Fe_0–F_1–Fe_2–F_{10}–Fe_{21} chains with $\widehat{FeFFe} \simeq 153°$ and $\widehat{FFeF} \simeq 180°$. It was also found that, despite general similarities between FeF_3 and ReO_3 crystallographic structures, the Fourier transforms of the XAFS signals at the Fe K and Re L_3 edges differ significantly beyond the first-shell peak, mainly due to differences in iron and rhenium scattering amplitudes and phases (the rhombohedral distortion becomes important only for outer shells located beyond 4 Å).

1. Introduction

It is well known that the multiple-scattering (MS) contribution to the x-ray absorption fine structure (XAFS) is very important in compounds having linear or near-linear atom chains [1–3]. The reason for this is a drastic increase in the MS signal amplitude when the photoelectron is scattered by an atom in the forward direction. This phenomenon is known as the 'focusing effect', and its origin is due to a large difference between back- and forward-scattering properties of atoms. Until now, the importance of the focusing effect was mainly emphasized either in the first shell for octahedral coordination [2–4] or in the second shell when the atoms located there form near-linear chains together with the first-shell atoms and the absorber [2, 3]. In the first case, the focusing effect is caused by the absorber located between two other atoms, while in the second case it takes place at the atoms of the first shell. Note that in both cases the MS signals are generated within *three-atom* chains. In this work we shall show, using the example of FeF_3, that in the presence of *many-atom* quasi-linear chains, an analogous effect, which we shall call 'superfocusing', can take place leading to an increase of the XAFS amplitude from distant shells (> 6 Å). In the standard analysis of XAFS, only the single, double and triple scatterings are usually considered. Since more than three atoms are involved in the superfocusing effect, the scattering processes of higher order than the triple one become important. In the particular case of FeF_3, the multiple-scattering signals up to eighth order should be included (see sections 3 and 4).

Iron fluoride FeF_3 has a rhombohedrally distorted ReO_3-like structure with space group $R\bar{3}c$ formed by FeF_6 octahedra joined by corners ($\widehat{FFeF} \simeq 180°$ and $\widehat{FeFFe} \simeq 153°$)

0953-8984/94/234395+10$19.50

with the iron atoms at the centre [5,6]. To our knowledge, only one work has been published regarding the XAFS study of FeF_3 [7], in which the first coordination shell of iron was analysed using the plane-wave single-scattering approximation with theoretical back-scattering amplitudes and phases taken from [8]. A comparison of the results for the first shell obtained in [7] with those from the present work and from x-ray [5] and neutron [6] powder diffraction is given in section 4.

The paper is organized as follows. In section 2 the experiment and the procedure of the XAFS treatment are briefly described. Section 3 is devoted to the method of the XAFS calculation based on the *ab initio* multiple-scattering approach. In section 4 the main results are presented and discussed. Section 5 contains the main conclusions.

2. Experimental details and data analysis

The x-ray absorption spectra (XAS) of the iron K edge in FeF_3 were measured in transmission mode at room temperature on the DCI EXAFS-3 beam line (LURE, France). The synchrotron radiation was monochromatized using the Si(311) double-crystal monochromator detuned by 50% for harmonic rejection. The intensity was measured by two ionization chambers filled with air at atmospheric pressure. The energy scale was calibrated at the Fermi level of metal iron $E_F = 7112\,eV$ [9]. The experimental spectra were recorded in the energy range 7000–8300 eV with a step 2.6 eV and an energy resolution ~ 1 eV. The sample was prepared from finely ground polycrystalline FeF_3 powder with the total thickness x resulting in the absorption jump $\Delta\mu x \simeq 3.0$ (μ is the absorption coefficient).

The experimental data were analysed by the EXAFS data analysis software package EDA [10]. The x-ray absorption coefficient $\mu(E) = \ln(I_0/I)$ was calculated from the intensities of the synchrotron radiation, measured by two ionization chambers, before (I_0) and after (I) the sample. The background contribution $\mu_b(E)$ was approximated by the Victoreen rule ($\mu_b = A/E^3 + B/E^4$) and subtracted from the experimental spectrum $\mu(E)$. The resulting absorption coefficient in the vicinity of the edge is shown in figure 1(*a*). Furthermore, the atomic-like contribution $\mu_0(E)$ was found, by a combined polynomial/cubic-spline technique, to have a precise removal of the XAFS signal zero-line, and the XAFS $\chi(E)$ was determined as $\chi(E) = (\mu - \mu_b - \mu_0)/\mu_0$. We converted $\chi(E)$ into a space of the photoelectron wavevector k, defined as $k = [(2m/\hbar^2)(E - E_0)]^{1/2}$ where $E - E_0$ is the photoelectron kinetic energy measured from the inner core photoemission threshold (vacuum level), which is the energy origin for the theoretical data calculated by MSXAS [11, 12]. The energy origin E_0 was located, according to the method utilized earlier by one of us [3], at the energy $E_0 = E_F + \phi$, where E_F corresponds to the left-hand side of the pre-edge peak, located at 7114 eV (figure 1(*a*)), and $\phi \simeq 4.5$ eV is the workfunction [13]. The XAFS signal $\chi(k)$ was multiplied by a factor k^2 to compensate for the decrease in its amplitude with increasing wavevector (figure 2(*a*)). Furthermore, the Fourier transforms (FT) of the XAFS $\chi(k)k^n$ ($n = 2, 3, 4, 5$) signals with a Gaussian window, centred at the midpoint of the data range $k = 0.25$–$15.5\,Å^{-1}$, were calculated (figure 2(*b*)), and the contributions from three regions, labelled in figure 2(*b*) by the letters A, B and C, were singled out by the back FT in the ranges 0.7–2.1 Å, 2.7–3.8 Å and 6.4–7.5 Å, respectively. Note that, normalized to the first peak maximum, the FT of the XAFS $\chi(k)k^n$ signals, calculated with different weight factors n, are similar in all R space. This means that both experimental XAFS and its FT (figure 2) have a very good signal-to-noise ratio defined by low experimental noise in XAS, as well as by good background μ_b and zero-line μ_0 removal.

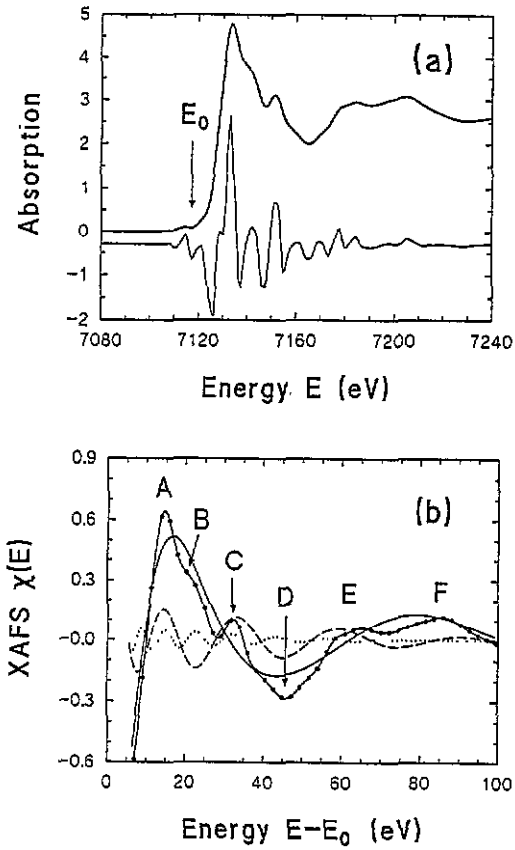

Figure 1. (*a*) X-ray absorption spectrum (XAS) of the iron K edge in FeF_3 and its second derivative. The position of the continuum threshold E_0 is also shown. (*b*) An enlarged part of the XAS shown in (*a*) (the full curve passing through full circles) with superimposed contributions from the main peaks in FT (figure 2(*b*)): 0.7–2.1 Å, 2.7–3.8 Å and 6.4–7.5 Å. The origin of the main features, labelled by letters, is discussed in the text.

3. Method of calculation

In multiple-scattering theory, the fine structure of the absorption coefficient $\chi(k)$ can be expanded in a series with the general form [14]

$$\chi(k) = \sum_n \chi_n(k) = S_0^2 \sum_n A_n(k, R_n^{ij}) \sin\left(kR_n + \Phi_n(k, R_n^{ij})\right)$$

where the sum is taken over all possible closed paths of order n ($n = 2, 3, \ldots$) giving the contribution $\chi_n(k)$ to the total signal $\chi(k)$; S_0^2 is the amplitude scaling factor reflecting the contribution of multi-electron processes, $A_n(k, R_n^{ij})$ and $\Phi_n(k, R_n^{ij})$ are the effective scattering amplitude and phase describing the interaction of the propagating photoelectron with the atoms included in the path, R_n is the total path length and R_n^{ij} is the length of the path from atom i to atom j. Note that the amplitude $A_n(k, R_n^{ij})$ depends, in addition to the scattering properties of atoms, upon the degeneracy of the path equal to the coordination number for the single-scattering signals, the photoelectron mean-free-path term $\exp\left(-R_n/\lambda(k)\right)$, and the Debye–Waller (DW) factor term $\exp(-2\sigma_n^2 k^2)$, reflecting both

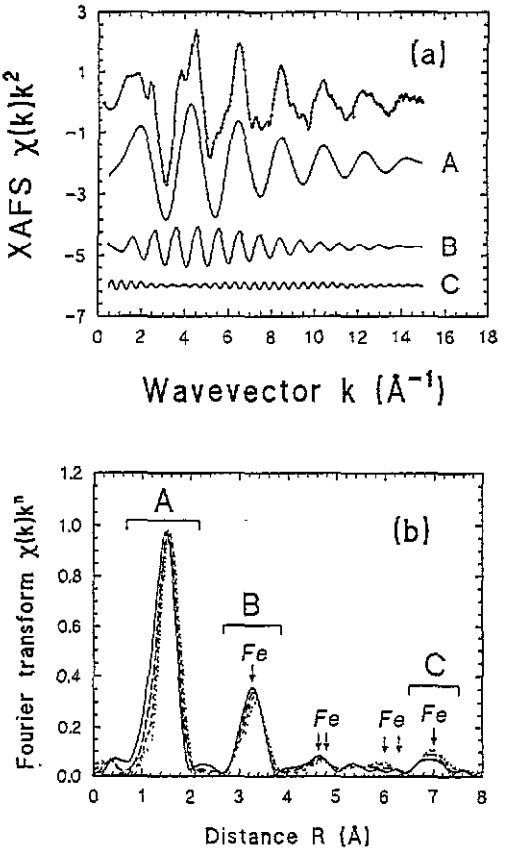

Figure 2. (*a*) Experimental XAFS $\chi(k)k^2$of the Fe K edge in FeF_3 (upper curve). The three signals A, B and C correspond to the contributions to the total XAFS from the three regions labelled in (*b*). (*b*) Fourier transforms of the experimental spectrum shown in (*a*) with different weight factors *n*: $n = 2$ (full curve), n=3 (long-dash broken curve), $n = 4$ (short-dash broken curve) and $n = 5$ (dotted curve). The positions of the shells containing iron atoms are shown by arrows. The curves are normalized to the first peak maximum. The peak positions are shifted from their true crystallographic values because the FT were calculated without phase correction.

static and thermal disorder effects. In the case of the MS signals, the treatment of the DW factor term in the exponential form is only approximate, since it ignores angular variations of scattering amplitudes and assumes only radial disorder. However, such an approach considered by us as a first approximation gives results in good agreement both in the amplitude and the phase with the experimental data for FeF_3 (see section 4). Note that the DW factors in our approach affect only the amplitude of the calculated signals.

In this work the *ab initio* multiple-scattering calculations of χ_n signals for $n = 2, \ldots, 8$ were performed using the MSXAS code [11, 12], based on the exact multiple-scattering theory described previously [14–17]. All parameters in the calculated spectra, except the DW factors, were taken in an *ab initio* way, while the DW factors for each MS path were set as free parameters [3]. The need to use different values of the DW factors for different MS paths is clear, since the DW factor depends on the number and type of scatterers composing the path and the anisotropy of their thermal vibrations. Therefore, even for paths generated within one chain of atoms, the values of the DW factors can be slightly different. Due to the

large number of the MS paths involved in the calculation of the XAFS signals corresponding to the peak B and, particularly, the peak C (figure 2(*b*)), we do not present here the DW factor values for each path. However, let us note that thermal damping decreases the amplitudes of these two XAFS signals by a factor of about two and three, respectively. The amplitude scaling factor S_0^2 was equal to one.

The total cluster potential and partial phase-shifts were calculated for a 27-shell cluster centred at the absorbing Fe_0 atom and consisting of 177 atoms inside a sphere of radius 8.1 Å. The details of the cluster potential calculation can be found in [14, 18]. Briefly, the total cluster potential was constructed from a set of spherically averaged *muffin-tin* (MT) potentials, which were built following the standard Mattheiss prescription [19]. The complex Hedin–Lundqvist (HL) potential, based on the density functional formalism within the single-plasmon pole approximation, was used to approximate the exchange-correlation term [14]. Thus the XAFS amplitude damping, associated with the inelastic losses of the photoelectron in extrinsic channels on plasmon excitations, was automatically included. The amplitude damping due to the core–hole finite lifetime was included through the empirically determined 1s(Fe) core-level width $\Gamma_K = 1.33$ eV [20]. The values of the MT radii were chosen according to the Norman criterion [21] with an overlap factor $\sim 10\%$, and were equal to 1.11 Å for iron and 1.00 Å for fluorine. The final state of the absorbing iron atom was taken to be fully relaxed with a hole localized in the 1s level.

4. Results and discussion

The near-edge XAFS of the Fe K edge in FeF_3 exhibit a complex structure, which is clearly visible in the second derivative of the absorption coefficient (figure 1(*a*)). A weak pre-edge peak, located below the photoemission threshold E_0 at 7115 eV, corresponds to the atomic-like transition from the deep 1s(Fe) core-level to the quasi-bound state with 3d(Fe) atomic character. This transition is forbidden in a perfect octahedron according to the dipole selection rule; therefore its small magnitude is probably due to the presence of slightly distorted FeF_6 octahedra [7] rather than due to strong p–d mixing of fluorine 2p and iron 3d orbitals, since the covalency of the Fe–F bonds in FeF_3 was found to be quite low [22]. The enlarged part of XAS beyond the threshold E_0 is shown in figure 1(*b*). There are six features, labelled by letters A–F, whose origin is due to photoelectron scattering by atoms located in outer coordination shells. The general shape is defined by the single-scattering signal (full curve) from six fluorine atoms in the first shell (the peak A in figure 2(*b*)). A fine structure (features A, C–F) appears due to the signal (broken curve) from iron atoms in the second shell and fluorine atoms in the third and fourth shells (the peak B in figure 2(*b*)). In addition, there is also a contribution (dotted curve) to the features A, B and C from distant shells located as far as ~ 7.0–8.0 Å from the absorber (the peak C in figure 2(*b*)).

The experimental XAFS $\chi(k)k^2$ ($k = 0.25$–15.0 Å^{-1}) and three signals A, B and C, related to the contributions from three regions in FT (figure 2(*b*)), are shown in figure 2(*a*). To exclude the influence of the Fourier filtering procedure, the analysis of the XAFS signals A, B and C was made in the range $k = 2.5$–14.0 Å^{-1}.

Since the structure of FeF_3 is similar to ReO_3, one can expect that their FT will also be similar. However, a large difference between them is clearly seen at distances $R > 2$ Å (the upper curves in figure 3). While the first peak, related to the first shell, is located in both compounds at a close position (~ 1.5 Å), the peak corresponding to the second shell is shifted in FeF_3 to a shorter distance (~ 3.3 Å) compared to ReO_3 (~ 3.5 Å). Furthermore, there is no peak at ~ 2.8 Å in FeF_3, while in ReO_3 it is well defined and corresponds to

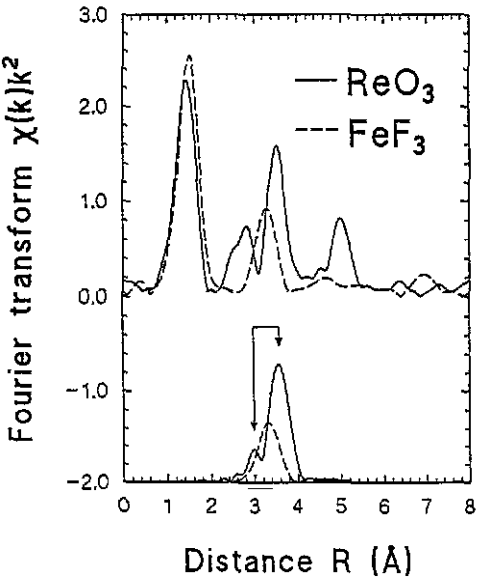

Figure 3. Fourier transforms of the rhenium L_3-edge (full curve) and iron K-edge (broken curve) XAFS $\chi(k)k^2$ in ReO_3 and FeF_3 (upper curves) and the single-scattering $\chi(k)k^2$ signals corresponding to the metal–metal pairs (lower curves). The data for ReO_3 are taken from [3]. Note the double-hump shape for the Re–Re signal (lower full curve) marked by arrows.

the MS contribution from the first coordination shell [2, 3]. The reason for such differences is easy to understand if one remembers the large separation of iron ($Z = 26$) and rhenium ($Z = 75$) atoms in the periodic table. The single-scattering contribution to the FT from rhenium atoms in the second shell has a double-hump shape [2, 3], which is typical for all heavy elements, whose left-hand side has a smaller amplitude and is shifted to shorter distances (lower full curve in figure 3). In contrast, iron atoms produce a single peak (lower broken curve in figure 3). Among MS signals in the first shell, the main contribution to the peak at ~ 2.8 Å is given by linear O–Re–O chains [2, 3] where the focusing effect at the central atom takes place, therefore the peak position is sensitive to the scattering phase of the rhenium atom. In the same way the MS signal in the first shell in FeF_3 is sensitive to the iron scattering phase. Thus the difference between the ReO_3 and FeF_3 FT in the range 2.0–4.0 Å is just a reflection of large differences in rhenium and iron scattering properties. The peak at 5 Å, which is present in the FT of ReO_3, is strongly spread in FeF_3. This fact can be explained with two points: (i) the difference in the scattering amplitudes of rhenium and iron atoms and (ii) the rhombohedral distortion of the perfect perovskite-like structure in FeF_3 [5, 6]. Due to the last fact, in contrast to ReO_3 where only one group of 12 rhenium atoms exists at 5.30 Å, in FeF_3 iron atoms are smeared into two groups of six atoms each located at 5.19 Å and 5.36 Å, whose positions in FT, shifted on ~ 0.5 Å due to the iron phase, are shown in figure 2(*b*) by arrows.

The best-fit parameters obtained in present work for the first coordination shell (the peak A in figure 2(*b*)), formed by six fluorine atoms, are compared with those from [5–7] in table 1. The present values are in better agreement with the results of x-ray [5] and neutron [6] powder diffractions than those from the previous XAFS study [7]. The determined value of the Fe–F distance, $R = 1.919$ Å, was utilized in the construction of the 27-shell cluster around the central iron atom using the symmetry operations of the $R\bar{3}c$ space group

Table 1. Room-temperature structural data obtained for the first coordination shell of iron in FeF_3 by XAFS (in the present work and in [7]), x-ray powder diffraction (XRPD) [5] and neutron powder diffraction (NPD) [6]. (N is the number of fluorine atoms, R is the interatomic Fe–F distance and σ is the Debye–Waller factor for the Fe–F pair.)

	XAFS	XAFS [7]	XRPD [5]	NPD [6]
N	6.00 ± 0.04	6.0 ± 1	6	6
R (Å)	1.919 ± 0.002	1.93 ± 0.01	1.92	1.923
σ (Å)	0.054 ± 0.007	0.05		

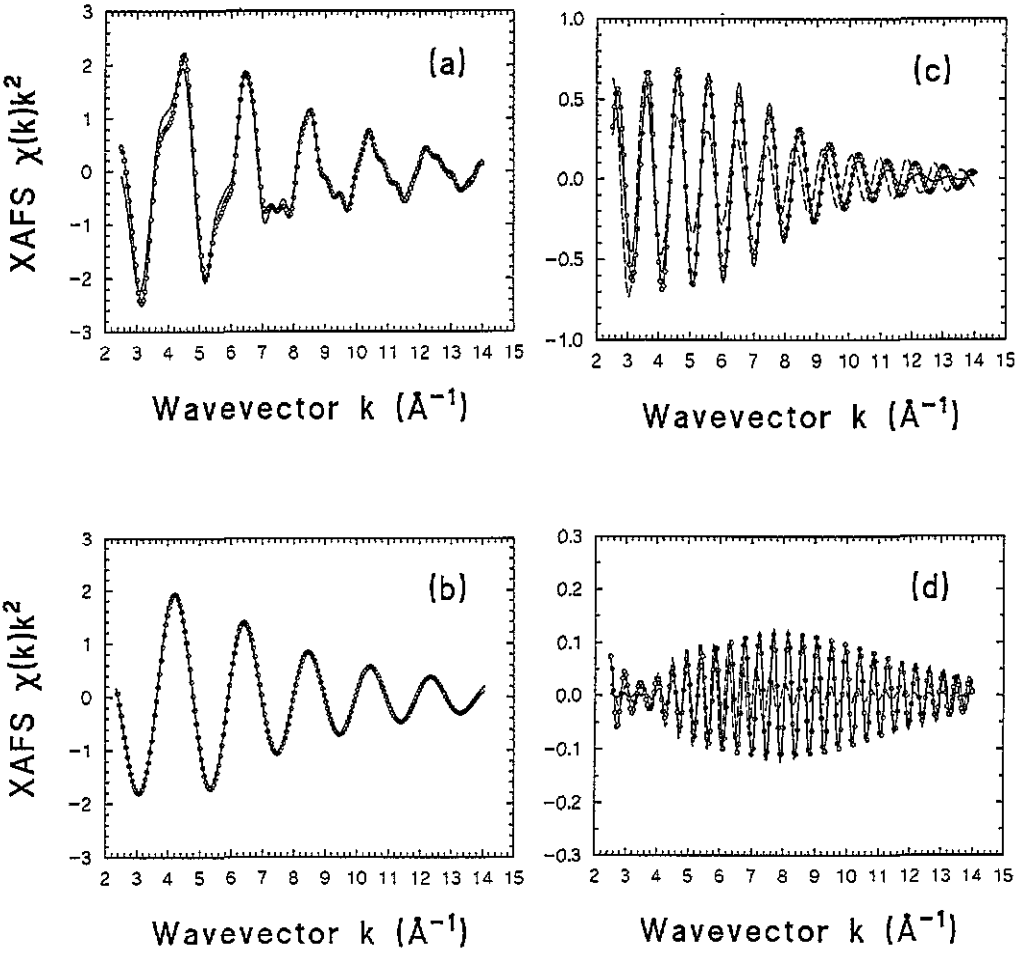

Figure 4. Comparison of experimental (circles) and calculated (full curve) XAFS signals $\chi(k)k^2$ corresponding to the total signal (*a*) and to the peaks A (*b*), B (*c*) and C (*d*) labelled in figure 2(*b*). The broken curve in (*c*) and (*d*) shows the single-scattering contribution.

and the fractional coordinates of atoms given in [6]. The calculated XAFS $\chi(k)k^2$ signals (total and separate contributions related to the peaks A, B and C) are compared with the experimental signals in figure 4. The total single-scattering contributions to the peaks B and C are also shown in figure 4(*c*) and (*d*) by broken curves. Good agreement has been found between calculated and experimental signals. It is clear that the MS contributions are very important in describing the XAFS signals from outer peaks (B and C); however,

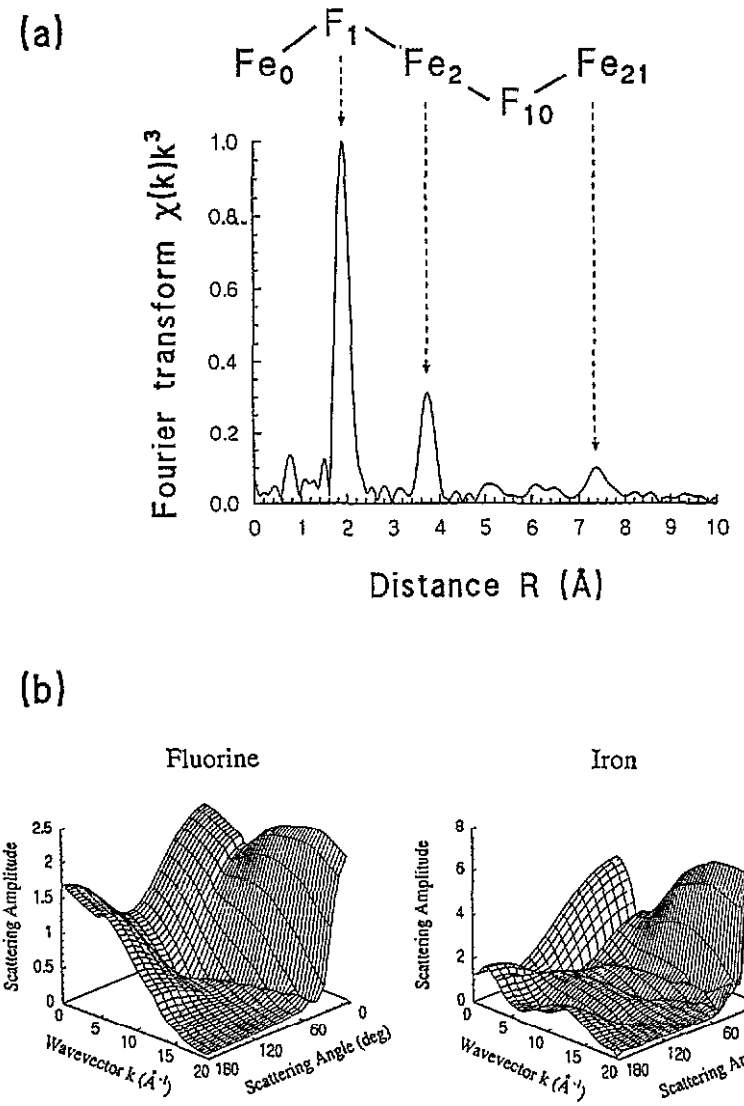

Figure 5. (*a*) Relation between the peaks in FT, corrected on the back-scattering amplitude and phase of iron and normalized to the first peak maximum, and atoms of the Fe_0–F_1–Fe_2–F_{10}–Fe_{21} chain with $\widehat{FeFFe} \simeq 153°$ and $\widehat{FFeF} \simeq 180°$, which is responsible for the superfocusing effect in the Fe K-edge XAFS in FeF_3. (*b*) The angular dependence of the atom scattering amplitude for fluorine and iron atoms. The angle $\theta = 0°$ corresponds to the forward-scattering process and $\theta = 180°$ to the back-scattering process.

among the large number of MS paths existing in the cluster, only a few of them give a significant contribution in the range of peaks B and C: they correspond to the MS signals generated within the Fe–F–Fe and Fe–F–Fe–F–Fe chains, respectively (figure 5(*a*)), and have an amplitude 30–200% of the single-scattering signal for the Fe–Fe atom pairs. The amplitude of the XAFS signal from iron atoms Fe_2 in the second shell is amplified due to the focusing effect within the Fe_0–F_1–Fe_2 chains (Fe_0 denotes the absorber, and the number is related to the coordination shell), caused by fluorine atoms F_1 of the first shell.

The contribution from iron atoms Fe_{21} (peak C), located as far as 7.5 Å, is observed due to the 'superfocusing' effect within the Fe_0–F_1–Fe_2–F_{10}–Fe_{21} chains with $\widehat{FeFFe} \simeq 153°$ and $\widehat{FFeF} \simeq 180°$. The superfocusing effect consists in the increase of the photoelectron wave amplitude as a result of several focusing effects which take place one by one. The origin of the focusing and superfocusing effects in the two above-mentioned chains in FeF_3, respectively, is easy to understand from the behaviour of iron and fluorine scattering amplitudes shown in figure 5(*b*). The scattering at the iron atom Fe_2 in the second chain always takes place in the forward direction with a scattering angle equal to 0°; therefore, the corresponding amplitude has a maximum value and increases with energy. The scatterings at the fluorine atoms F_1 and F_{10} are in a less linear direction with a scattering angle equal to $27° (= 180 - \widehat{FeFFe})$; however, the corresponding amplitude is also large enough and slowly decreases with energy. Since the total effective amplitude of the XAFS signal $A_n(k, R_n^{ij})$ is proportional to the product of the scattering amplitudes of all atoms participating in the scattering process [23], the product will grow for both chains, and $A_n(k, R_n^{ij})$ will be damped only by the path length (the factor $1/R^2$) and the Debye–Waller and mean-free-path terms. In the general case the competition between the latter effects and the product of the scattering amplitudes can lead to a decrease or increase of the signal amplitude, depending upon which effect dominates. In particular, in the case of FeF_3 both scattering amplitudes of iron and fluorine atoms have maxima in similar energy regions (figure 5(*b*)) due to the fact that the amplitude damping is not very strong and the signal from the Fe_0–F_1–Fe_2–F_{10}–Fe_{21} chains can be detected in spite of large distance and disorder effects.

5. Summary and conclusions

We have presented an *ab initio* multiple-scattering analysis of the Fe K-edge x-ray absorption fine structure in FeF_3. It has been found that the MS contributions from Fe–F–Fe and Fe–F–Fe–F–Fe chains, associated with 'focusing' and 'superfocusing' effects, are very important for the interpretation of XAFS data. We have also shown that the difference in scattering amplitudes and phases can lead, in the case of compounds with similar crystallographic structures such as FeF_3 and ReO_3, to a drastic modification of their XAFS signals.

Acknowledgments

One of us (AK) is grateful to Professor C R Natoli and co-workers (Laboratori Nazionali di Frascati) for use of the MSXAS code. AK also wishes to thank Dr M Hofmann (Institut für Anorganische Chemie I, Tübingen) for providing the FeF_3 powder, and to acknowledge the hospitality of the Università di Trento (Professor G Dalba) where part of this work was done.

References

[1] Lee P A and Pendry J B 1975 *Phys. Rev.* B **11** 2795
[2] Kuzmin A and Purans J 1993 *J. Phys.: Condens. Matter* **5** 267
[3] Kuzmin A, Purans J, Benfatto M and Natoli C R 1993 *Phys. Rev.* B **47** 2480
[4] Garcia J, Sanchez del Rio M, Burattini E, Benfatto M and Natoli C R 1989 *Physica* B **158** 409
[5] Hepworth M A, Jack K H, Peacock R D and Westland G J 1957 *Acta Crystallogr.* **10** 63
[6] Leblanc M, Pannetier J, Ferey G and De Pape R 1985 *Rev. Chim. Miner.* **22** 107

[7] Greneche J M, Le Bail A, Leblanc M, Mosset A, Varret F, Galy J and Ferey G 1988 *J. Phys. C: Solid State Phys.* **21** 1351
[8] Teo B K and Lee P A 1979 *J. Am. Chem. Soc.* **101** 2815
[9] Bearden J A and Burr A F 1967 *Rev. Mod. Phys.* **39** 125
[10] Kuzmin A 1993 *EDA: EXAFS Data Analysis Software Package* User Manual (unpublished)
[11] Ruiz-López M F, Bohr F, Filipponi A, Di Cicco A, Tyson T A, Benfatto M and Natoli C R 1991 *Proc. 6th Int. Conf. on X-ray Absorption Fine Structure (York)* ed S S Hasnain (Singapore: Ellis Horwood) p 75
[12] Tyson T A 1991 *PhD Thesis* Stanford University
[13] Eastman D E 1970 *Phys. Rev.* B **2** 1
[14] Tyson T A, Hodgson K O, Natoli C R and Benfatto M 1992 *Phys. Rev.* B **46** 5997
[15] Natoli C R and Benfatto M 1986 *J. Physique Coll.* **47** C8 11
[16] Benfatto M, Natoli C R, Brouder C, Pettifer R F and Ruiz-López M F 1989 *Phys. Rev.* B **39** 1936
[17] Brouder C, Ruiz-López M F, Pettifer R F, Benfatto M and Natoli C R 1989 *Phys. Rev.* B **39** 1488
[18] Ruiz-López M F, Loops M, Goulon J, Benfatto M and Natoli C R 1988 *Chem. Phys.* **121** 419
[19] Mattheiss L F 1964 *Phys. Rev.* A **134** 970
[20] Keski-Rahkonen O and Krause M O 1974 *At. Data Nucl. Data Tables* **14** 139
[21] Norman J G 1974 *Mol. Phys.* **81** 1191
[22] Jacobson A J, McBride L and Fender B E F 1974 *J. Phys. C: Solid State Phys.* **7** 783
[23] Rehr J J and Albers R C 1990 *Phys. Rev.* B **41** 8139